

Chapter 1

Quasicrystals

The discovery of a quasicrystalline phase in a rapidly cooled Al-Mn alloy [1] broke the fundamental concept of crystallography because the diffraction of the alloy had a sharp diffraction pattern with a rotational symmetry incompatible with periodicity. This new finding forced a reconsideration of the traditional definition of a crystal as *a periodic arrangement of identical unit cells*. In 1992, the International Union of Crystallography redefined crystals as *any solid having an essentially discrete diffraction diagram* [34].

Periodic crystals are formed by a periodic repetition of a single building block the so-called unit cell exhibiting a long range translational and orientational symmetry. Only 2-, 3-, 4-, and 6-fold non-trivial rotational symmetries are allowed in the periodic crystals and their diffraction patterns give sharp Bragg peaks reflecting the symmetry and long range order.

In contrast to periodic crystals, quasicrystals exhibit a long range order in spite of their lack of translational symmetry and often possess n -fold ($n = 5$ and > 6) rotational symmetries. Most of the quasicrystalline structures can be described by using quasiperiodic tiling models [35, 36], where two or more different ‘unit cells’ (tiles) are used as the building blocks of the structure. An alternative model is a covering model, where a single, overlapping tile acts as unit cell [37].

The diffraction pattern of quasicrystals shows a dense set of Bragg peaks with their positions related by the irrational number $\tau = 1.618\dots = 2 \cos \frac{\pi}{5}$, the so-called golden mean, which is related to the geometry of pentagonal and decagonal symmetries. In contrast to periodic crystals, where three integer indices are sufficient to characterize the diffraction of a 3D structure, n integer indices ($n > 3$) are required to generate the diffraction vectors of aperiodic crystals

indicating that the spots could be related to a nD periodic lattice. In fact, quasicrystals of all kinds can be explained by periodic lattices in higher dimensional space.

This chapter includes a discussion about the basic concepts, stability and structure models of quasicrystals followed by structural details of d -Al-Ni-Co.

1.1 Basic Concepts

1.1.1 Basic Types of Quasicrystalline Lattices

Fibonacci Sequence

The Fibonacci sequence is a fundamental and a well-known example of a 1D quasiperiodic structure exhibiting aperiodic long range order. Although it does not feature orientational symmetry, the Fibonacci sequence illustrates many important properties of quasicrystals, which can be generalized to 2D and 3D quasicrystals. The Fibonacci sequence is built from two elements ‘L’ (large) and ‘S’ (small). The sequence can be generated by a substitution rule $L \rightarrow LS$ and $S \rightarrow L$. The resulting sequence is as follows:

Generation	Fibonacci Sequence	Fibonacci Number
1 st	L	1
2 nd	LS	2
3 rd	LSL	3
4 th	LSLLS	5
5 th	LSLLSLSL	8
6 th	LSLLSLSLLSLLS	13
...	so on	

The frequencies of ‘L’ and ‘S’ in each sequence and the ratio of successive Fibonacci number (number of line segments in each generation) is τ (the golden mean) in the limit of infinite sequence length. The sequence is self-similar. This implies that inflation or deflation of a Fibonacci sequence yields another Fibonacci sequences with different length segment. The sequences can be generated by taking a single line segment and applying the deflation rule ($L_n \rightarrow L_{n+1}S_{n+1}$ and $S_n \rightarrow L_{n+1}$, n denotes number of generations) with an additional constraint that the ratio of line segments in each generation is equal to the golden mean i.e. $\frac{L_n}{S_n} = \tau$. Furthermore, the

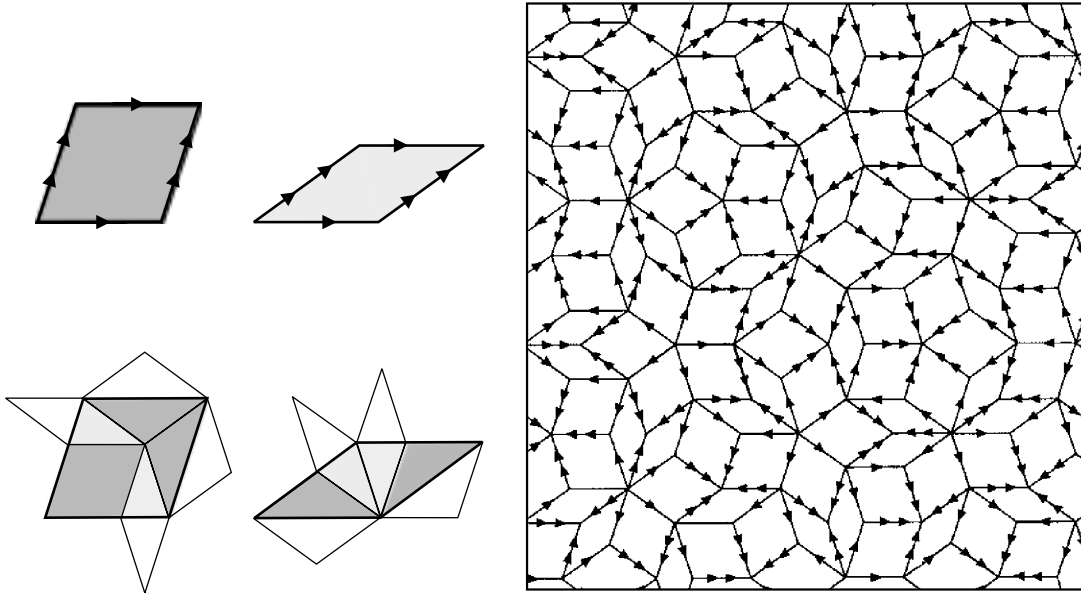


Figure 1.1: A rhombic Penrose pattern (right panel) generated by two rhombi (left upper panel). The lower left panel shows the deflating scheme.

diffraction of the Fibonacci sequence gives sharp Bragg peaks with many interesting features, which will be discussed in the next section.

Penrose Tiling: A 2D Quasicrystalline Lattice

In 1974 the British mathematician Roger Penrose found that the 2D plane can be covered in a non-periodic fashion with two types of rhombi with equal edge length [38]. The importance of the Penrose tiling in solid state physics was realized only after the discovery of quasicrystals in 1984. Indeed, the Penrose pattern gives a diffraction pattern very similar to the diffraction observed from decagonal QCs [39].

Figure 1.1 shows a 2D rhombic Penrose pattern generated by two types of rhombi, one with an angle of 36° (skinny rhombus) and another with an angle of 72° (fat rhombus) (also see Figure 1.9). A perfect quasiperiodic pattern can be obtained only if the tiles are packed with a specific matching rule. The rule is simple, two rhombi are allowed to join if the arrows in their common edge match [38].

The Penrose pattern possesses many interesting features. Both areas and frequencies of skinny and fat rhombi in the pattern are of a ratio $1 : \tau$. The pattern consists of five sets

of tile-edges each parallel to the sides of a regular pentagon. The edges belonging to each set are orientated along a Fibonacci grid (a Fibonacci grid is a set of parallel lines separated by distances forming a Fibonacci sequence). This gives evidence of the long range order of the Penrose pattern. Furthermore, the local 5-fold and 10-fold rotational symmetries can be observed in the pattern. Some of decagonal and pentagonal features are highlighted in Figure 1.9.

Another important feature of the tiling is its self-similarity. A Penrose pattern can be transformed to another Penrose pattern by deflating/inflating the skinny and fat rhombi. Figure 1.1 (left lower panel) shows the deflating scheme, where the fat and skinny rhombi are divided into smaller fat and skinny rhombi. The fat rhombus is divided into two fat and one skinny rhombus, while the skinny rhombus is divided into one fat and one skinny rhombus. The area of the new fat and skinny rhombi is smaller than the respective old rhombi by a factor of τ^2 . Starting from a single rhombus, an arbitrarily large section of a Penrose tiling can be produced by continuously applying the deflation rule. There are some other 2D quasicrystalline tilings such as the pentagonal Penrose tiling (Figure 1.9) and the octagonal Penrose tiling, which explain the diffraction pattern of other polygonal QCs [40]. The idea of space filling is extended to 3D space, where two kinds of rhombohedrons are needed to fill the 3D space aperiodically [41]. The Fourier transform of the 3D Penrose tiling explains the diffraction pattern observed in icosahedral QCs [42, 43].

1.1.2 Higher Dimensional Concept

Higher dimensional crystallography was first introduced by de Wolff in 1974 [44]. Many quasiperiodic structures can be considered as a physical space projection or irrational cut of a higher dimensional periodic lattice. For instance, 2D and 3D Penrose tilings can be obtained from 4D and 6D periodic space, respectively [45]. Rotational symmetries incompatible with 3D periodicity are allowed in suitable nD ($n > 3$) periodic space. The body diagonal of a hypercubic lattice in nD space, for example is an n-fold rotational axis.

In this section, a method to generate 1D and 2D quasicrystalline lattices is presented. There are two procedures to derive quasicrystalline lattices from higher dimension: (a) the projection method, and (b) the section or embedding method, also called the cut method. The section method is dealt in the following because it provides a convenient way to obtain the diffrac-

tion pattern and the quasicrystalline structure can be explained in term of symmetry, lattice parameter and unit cell distributions in higher dimensional periodic space.

Fibonacci Sequence Generated from the 2D Square Lattice by the Section Method

Let us consider a 2D square lattice (lattice constant a) with a set of axes X_{\perp} and X_{\parallel} rotated by an angle α with respect to the axes of the square lattice (Figure 1.2(a)). The lattice is decorated with line segments A_{\perp} of length $\Delta = a(\cos \alpha + \sin \alpha)$ with the orientation along the X_{\perp} -axis. The point of intersection of the A_{\perp} with the X_{\parallel} -axis yields a Fibonacci lattice if the slope of X_{\parallel} -axis is the reciprocal of the golden mean, i.e., $\cot \alpha = \tau$. This process of getting quasicrystalline structures from higher dimension periodic decorated lattices is called the section method. The line segment used to decorate the higher dimensional lattice is called the atomic surface or occupation domain or hyperatom. The X_{\parallel} -axis locating the quasicrystalline lattice is called parallel space or physical space or external space, while its perpendicular counterpart along which the atomic surface is situated is called internal or perpendicular space.

The diffraction pattern of the Fibonacci sequence is calculated now. The distribution of lattice points in a 2D square lattice can be expressed by,

$$\rho(\mathbf{r}) = \sum_{m,n} \delta(\mathbf{r} - ma\mathbf{e}_x - na\mathbf{e}_y). \quad (1.1)$$

The Fourier transform of $\rho(\mathbf{r})$ is a square lattice with lattice spacing of $\frac{2\pi}{a}$. It can be written as,

$$F(\mathbf{Q}) = \frac{1}{a^2} \sum_{hh'} \delta(\mathbf{Q} - \mathbf{Q}^{hh'}), \quad (1.2)$$

where $\mathbf{Q}^{hh'}$ are vectors of the reciprocal lattice, which have two components $\frac{2\pi}{a}h$ and $\frac{2\pi}{a}h'$ along X^* - and Y^* -axes (X^* and Y^* are the reciprocal space axes associated with the real space axes X and Y , respectively). The $\mathbf{Q}^{hh'}$ can be decomposed into the parallel and perpendicular space components, i.e. $\mathbf{Q}^{hh'} = (Q_{\parallel}^{hh'}, Q_{\perp}^{hh'})$ with,

$$Q_{\parallel}^{hh'} = \frac{2\pi}{a} \sqrt{\frac{\tau^2}{\tau^2 + 1}} \left(h + \frac{h'}{\tau} \right), \quad (1.3)$$

and

$$Q_{\perp}^{hh'} = \frac{2\pi}{a} \sqrt{\frac{\tau^2}{\tau^2 + 1}} \left(h' - \frac{h}{\tau} \right). \quad (1.4)$$

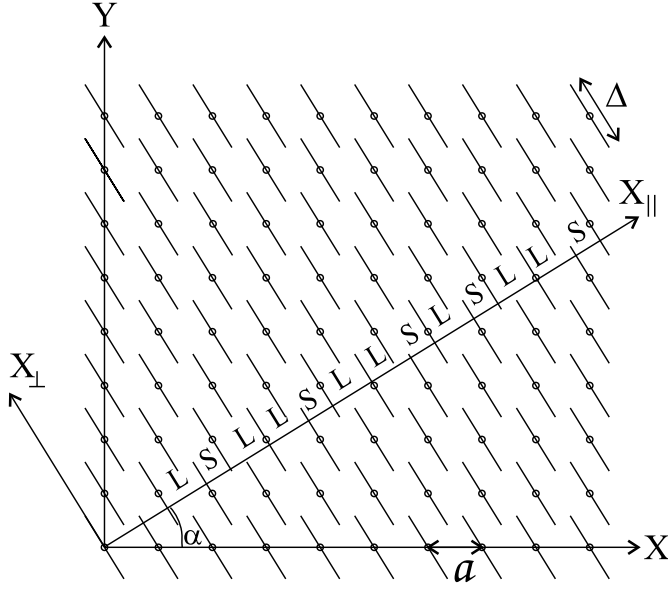


Figure 1.2: (a) The section method generating a Fibonacci sequence from a 2D square lattice decorated with line segments.

The density distribution of the decorated periodic lattice $\rho'(\mathbf{r})$ is the convolution product of $\rho(\mathbf{r})$ with A_{\perp} , i.e.,

$$\rho' = \rho * A_{\perp}. \quad (1.5)$$

The Fourier transform of $\rho'(\mathbf{r})$ is given by the product of the Fourier transforms of ρ and A_{\perp} ,

$$F'(\mathbf{Q}) = \left[\frac{1}{a^2} \sum_{hh'} \delta(\mathbf{Q} - \mathbf{Q}^{hh'}) \right] G(Q_{\perp}), \quad (1.6)$$

where $G(Q_{\perp})$ is the Fourier transform of A_{\perp} and given by,

$$G(Q_{\perp}) = \Delta \frac{\sin(Q_{\perp} \Delta / 2)}{(Q_{\perp} \Delta / 2)}. \quad (1.7)$$

The main idea of the section method is that the cut operation is performed in real space, while the projection is carried out in the reciprocal space. This method uses the fact that the Fourier transform of a projection is a cut and vice versa. Thus, the density distribution of the Fibonacci lattice $\rho(r_{\parallel})$ is obtained by the cut of $\rho'(\mathbf{r})$ by X_{\parallel} , while its Fourier components are evaluated by the projection $F'(\mathbf{Q})$ on X_{\parallel}^* . The Fourier components of the Fibonacci lattice thus can be written as,

$$F'(Q_{\parallel}) = \frac{1}{a^2} \sum_{hh'} [\delta(Q_{\parallel} - Q_{\parallel}^{hh'}) G(Q_{\perp}^{hh'})], \quad (1.8)$$

The presence of the δ -term implies that the diffraction pattern of the Fibonacci lattice exhibits sharp Bragg peaks. The intensity of the diffraction peaks associated with (h, h') is given by,

$$I_{hh'} = |G(Q_{\perp}^{hh'})|^2 = \Delta^2 \frac{\sin^2(Q_{\perp}^{hh'} \Delta / 2)}{(Q_{\perp}^{hh'} \Delta / 2)^2}, \quad (1.9)$$

The intensity is maximized when $\frac{h}{h'} \rightarrow \tau$ (ratio of successive Fibonacci number). The strong diffraction peaks thus take indices having the ratio approximately equal to τ .

Many features important for quasicrystals can be extracted from the diffraction vector $Q_{\parallel}^{hh'}$ of the Fibonacci lattice (Equation 1.3). Firstly, the diffraction peaks are indexable with two indices h and h' (which are the Miller indices of the 2D square lattice) even though the structure is 1D. Secondly, the diffraction vector produces an aperiodic reciprocal lattice because of an irrational coefficient of h' . Thirdly, since $Q_{\parallel}^{hh'}$ is invariant under multiplication of τ^n , there is no restriction of minimum separation between the diffraction spots. (The invariance can be illustrated by taking an arbitrary value of n , say $n = 1$ for simplicity, then $Q_{\parallel}^{hh'} \times \tau = \frac{2\pi}{a} \sqrt{\frac{\tau^2}{\tau^2+1}} (h + \frac{h'}{\tau}) \times \tau = \frac{2\pi}{a} \sqrt{\frac{\tau^2}{\tau^2+1}} (h\tau + h') = \frac{2\pi}{a} \sqrt{\frac{\tau^2}{\tau^2+1}} (h(\frac{1}{\tau} + 1) + h') = \frac{2\pi}{a} \sqrt{\frac{\tau^2}{\tau^2+1}} (h + h' + \frac{h}{\tau}) = \frac{2\pi}{a} \sqrt{\frac{\tau^2}{\tau^2+1}} (\tilde{h} + \frac{h}{\tau}) = Q_{\parallel}^{h\tilde{h}}$ with $\tilde{h} = h + h'$).

Penrose Tiling Generated from 4D Space

A 2D rhombic Penrose tiling can be obtained from 4D periodic space, which can be decomposed into a 2D physical space V^{\parallel} and a 2D perpendicular space V^{\perp} . The unit cell of the 4D lattice is decorated with five types of pentagonal atomic surfaces [39, 45] orientated parallel to V^{\perp} . The atomic surfaces intersect V^{\parallel} at points generating the vertices of the rhombic Penrose tiling. The Penrose patterns of other variants are obtained by taking different types of atomic surfaces. For example, a pentagonal Penrose pattern is obtained by a single decagonal atomic surface. The section method to generate a periodic stacking of the pentagonal and rhombic Penrose tilings from a 5D space will be discussed later in Section 1.3.3.

1.1.3 Phasons and Approximants

The higher dimensional description of the quasicrystals introduces additional degrees of freedom related to perpendicular space. The ordinary elastic excitation in quasicrystals is characterized by phonons, which involves the translation of atoms in physical space. In contrast, the elastic excitation associated with the new degrees of freedom corresponds to the translation of the atomic surfaces along the perpendicular space. The associated elementary excitations are called phasons. Since the perpendicular space does not exist in reality, only the effects of phason excitation in the physical space are relevant in practice. The phason excitations cause atomic jumps in the physical space in contrast to the phonon excitations which result in a collective

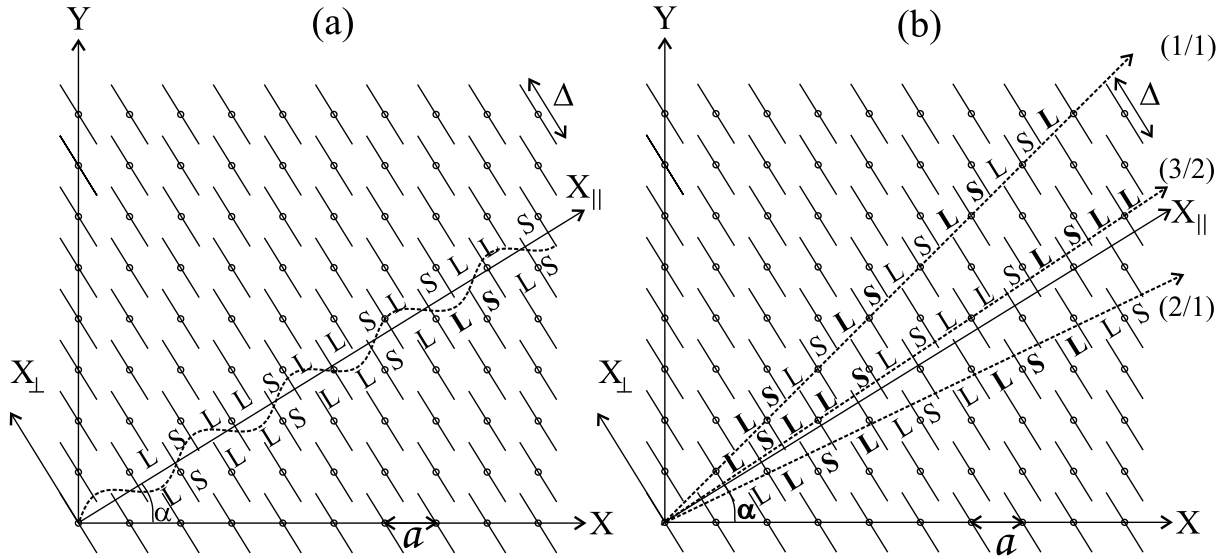


Figure 1.3: An illustration of phason-disorder (a) and approximants of a Fibonacci sequence generated by employing uniform phason strain rotating the physical space X_{\parallel} .

continuous motion of atoms. A very simple example illustrating how phasons influence the structure in the physical space is presented below.

Consider once again the section method generating a Fibonacci sequence (Figure 1.3(a)). Assume the atomic surfaces are displaced along X_{\perp} due to the phasonic excitations and the displacement is defined by a sinusoidal function (for the sake of simplicity, the physical space is sliced by a curve represented by the sinusoidal function in the figure). The displacement of atomic surfaces results in a new sequence **LLSLSLLSLLSLS**..., where some of the tiles (written in bold characters) have been rearranged as compared to the original sequence **LLSLLSLLS**.... The rearrangement of tiles in real quasicrystals corresponds to atomic jumps between different positions, which are normally referred to as phason-flips. Indeed, the atomic jumps has been experimentally observed by transmission electron microscopy [46]. At low temperatures, the phason-flips are trapped as defects (phason disorder).

Both phonon and phason disorder influence the diffraction pattern. While the presence of phonons decreases the diffraction intensities via the conventional Debye-Waller factor yielding background intensity, the phasons decrease the intensities via a phasonic Debye-Waller factor [47]. The phonon and phason Debye-Waller factors are dependent on Q_{\parallel} and Q_{\perp} , respectively. The phonons constitute small displacements of the atoms from their equilibrium position and

the average structure maintains a long range order. In contrast, phasons may break down the long range order and thus result not only in decreased intensities but also broaden the peaks, or even shift the peak position depending upon the nature of phason disorders (see Ref. [48, 49]).

Phasons are believed to play an important role in the formation of quasicrystals and in the phase transition between crystalline and quasicrystalline phases of an alloy. Let us present a simple example illustrating a transformation of a quasicrystalline structure into a periodic structure via a special phason strain. Consider the physical space rotated due to a phason strain such that the new slope is a rational number, which approximates the initial slope $1/\tau$ (Figure 1.3 (b)). The new slope may be $1/1$, $1/2$, $2/3$, $3/5$, or $5/8 \dots$ (ratio of successive Fibonacci numbers). The intersection of the rotated physical space with the atomic surfaces results in a periodic sequence. For example, an X_{\parallel} -axis with a slope of $2/3$ cuts the atomic surfaces yielding the sequence **LSLLSLSLLSLSLLSL**..., which has a periodic repetition of **LSLLS**. The resulting sequence is known as the $3/2$ rational approximant of the Fibonacci sequence. Similarly, $1/1$, $2/1$, $5/3$, and $8/5$ rational approximants of the Fibonacci sequence are **LSLSLSLSLSLSLSLSLS**..., **LLSLLSLLSLLS**..., and **LSLLSLSLLSLLSLSL** ... with repeating unit cells **LS**, **LSL**, and **LSLLSLSL**, respectively, revealing that the higher the order of the approximant the more similar it is to the corresponding quasicrystalline structure. The approximants are useful to model the local structure and to determine the physical properties of quasicrystals (see Ref. [50] for a review).

1.2 Stability and Structural Models

One and a half decades have passed since the discovery of quasicrystals with a tremendous effort to find a cause behind the physical origin of quasicrystals. There are two distinct approaches proposed so far to explain the stability of quasicrystals. The first approach is based on an energetic stabilization, the second on an entropic stabilization [49]. Depending on the specific quasicrystalline phase, one of these approaches reflects the dominant mechanism of stability. Similarly, different structural models have been proposed to explain the unique properties of quasicrystals.

Energetic and Entropic Stabilization

The energetic stabilization of quasicrystals can be interpreted in terms of a perfect Penrose tiling picture. The key idea is that the edge-matching rules of the Penrose tiling could reflect local rules to attain a minimal binding energy. However, many quasicrystals are stable only at high temperature and convert into crystalline phases at low temperature [51, 52]. One should thus expect that entropy may be responsible for stabilizing the quasicrystalline phases. The entropic stabilization can be described in terms of random tilings. The basic idea of the random tilings is that the edge-matching rules of the Penrose tiling are completely discarded and the tiles are allowed to join randomly to fill the space without gaps. The randomness induces topological disorder (topological entropy) in the system. The randomization of tilings may not be the only source of entropy. The entropy can be induced by chemical disorder (chemical entropy). If the chemical entropy is dominant, the structure can be topologically ordered even at high temperature. Joseph *et al.* have shown theoretically that Ni-rich *d*-Al-Ni-Co with a perfect tiling is stable only above 800 °C [53], which is also confirmed experimentally [54, 55].

Electronic Stabilization

An alternative possibility to explain the energetic stability of quasicrystals may be electronic stabilization. Electronic properties and stoichiometry observed in many quasicrystals indicate that a Hume-Rothery type mechanism of intermetallic compounds may play an important role in the stability of quasicrystals [3, 56]. The Hume-Rothery mechanism states that a specific structure of alloy is formed for a fixed effective density of valence electrons (e/a , electron-per-atom ratio) in such a way that the Fermi surface matches the Brillouin zone boundary opening a pseudo gap [57, 58], which lowers the energy of the system.

In fact, almost all stable icosahedral quasicrystals are found to have a specific value of e/a (~ 2.1 for the Zn-Mg-Al class and ~ 1.75 for the Al-TM class, where TM refers to transition metals) [3] satisfying the condition of gap opening at Fermi level, i.e., $Q = 2k_F$ (where Q is the magnitude of reciprocal lattice vector and k_F the radius of the Fermi sphere) [3, and find references therein]. In many quasicrystals, a pseudogap at the Fermi level has been observed theoretically and experimentally [2, and find references therein] supporting the Hume-Rothery type mechanism for many icosahedral phases. Although the value of e/a is fixed for icosahedral

quasicrystals, it varies in a significant wide range for decagonal quasicrystals [3].

Perfect Quasiperiodic Tiling Model

Geometrically constructed quasiperiodic tilings show many features similar to those observed in quasicrystals such as non-crystallographic orientational symmetry and perfect long range. The tiling is a suitable starting point in modeling the structure of quasicrystals. In a structural model based on a rhombic Penrose tiling, atoms are organized into two distinct clusters or tiles, the skinny and fat rhombi. The edge-matching rules of the Penrose tiling could be enforced by the energetic preference of parts of clusters to properly match across tiling edges.

Random Tiling Model

In the random tiling model, two different types of tiles are considered as basic building blocks as in the perfect tiling model. But unlike in the perfect tiling model, where a strict edge-matching rule is followed, the random tiling model allows the tiles to join their edges randomly, keeping the occurrence frequencies fixed due to fixed concentration of elements in the alloy. Obviously, randomness allows to form several degenerate states (configurations) including ones that are periodic and disordered. Henley has shown that the state (configuration) having maximum entropy has an average decagonal symmetry and a long range quasiperiodic order [59].

Most quasicrystals exhibit some degrees of disorder. Extremely few quasicrystals, in particular the Ni-rich phase of *d*-Al-Ni-Co, are known to reveal almost a perfect quasiperiodic ordering [54, 60, 61]. Therefore, the random tiling model is appropriate for the majority of quasicrystalline phases. This model also accounts for the experimentally observed diffuse scattering, as the diffraction pattern of the random tilings have sharp Bragg peaks in addition to some diffuse background [47].

Cluster Model

An alternative picture of quasicrystals is the covering picture. A single repeating cluster can be used to cover the space in quasiperiodic order, provided that the clusters can overlap or neighboring clusters can share the atoms (first introduced by Burkov in 1991) [62]. In the cluster model, the formation of quasicrystals can be explained in a similar fashion as the periodic crystal

in the sense that only a single type of low energy cluster is used to close-pack a macroscopic structure. The cluster is analogous to the unit cell in a periodic crystal, hence termed ‘quasi-unit cell’ and the cluster model is sometimes called quasi-unit cell model.

Indeed, clusters of decagonal shape have been observed in high-resolution transmission electron microscopy (HRTEM) in many decagonal phases [63, and find references therein], and most of the theoretical structural models of the decagonal quasicrystals are also based on a single decagonal overlapping cluster [55, 62, 64-69]. Similarly, icosahedral quasicrystals are believed to be made up of Mackay clusters [63]. Scanning tunneling microscopy of 2-fold and 5-fold surfaces of *i*-Al-Pd-Mn shows the aggregation of Mackay-type clusters [14, 15]. Furthermore, the cluster approach is suitable to interpret some physical properties of quasicrystals, especially the dynamical properties of *i*-Al-Pd-Mn and *d*-Al-Ni-Co measured by Neutron scattering [70-72] and electrical and thermal properties [73, and find references therein].

The cluster picture of decagonal quasicrystals is very closely related to the Penrose tiling picture. It has been shown that a rhombic Penrose tiling can be equivalently produced by using a single decagonal tile with an overlapping rule, instead of edge-matching rule [37, 74, 75]. Further developments have been made by H. C. Jeong and P. J. Steinhardt in this respect [37, 75]. They have shown that a perfect Penrose tiling can be uniquely produced by maximizing the density of some suitably chosen atomic clusters having minimum energy configuration, discarding the overlapping rules. These clusters are in a one-to-one correspondence with the decagonal cluster. This new approach is physically relevant to explain the formation of quasicrystals because the constraint of cluster overlapping rules or the constraint of atomic decoration of the clusters does not have to be considered.

The concept of random tiling can be introduced also in the cluster approach. Some constraints of the cluster overlapping rules of the perfect quasiperiodic covering are abandoned to yield a randomly ordered quasiperiodic structure (refer to [76] for details). The resulting structure is entropically stabilized similarly as the random tilings.

1.3 Decagonal Quasicrystals

Soon after the discovery of icosahedral quasicrystals, varieties of 2D quasicrystals were found (see [3, 77] for review). The 2D quasicrystals have periodic ordering along one direction and qua-

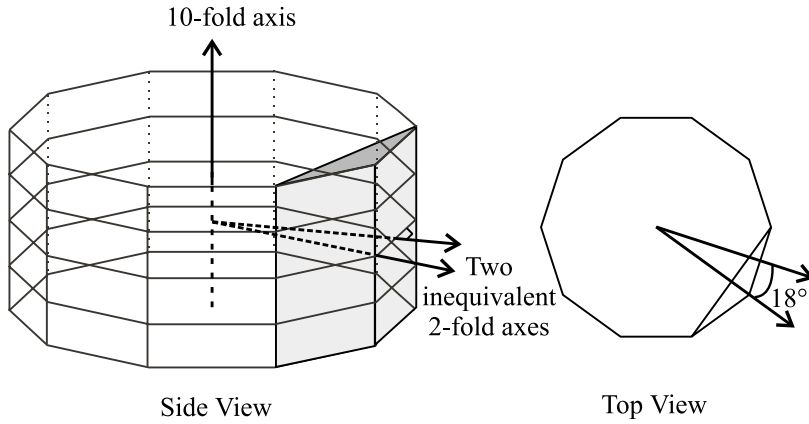


Figure 1.4: A macroscopic view of decagonal quasicrystal, which is formed by a periodic stacking of quasiperiodic planes along the 10-fold axis. Two inequivalent 2-fold planes perpendicular to the 10-fold planes are shaded.

sicrystalline ordering in the plane perpendicular to the periodic direction. The quasicrystalline plane can possess pentagonal, octagonal, decagonal, or dodecagonal symmetry. The influence of both quasicrystalline and crystalline ordering on the physical properties of quasicrystals can be investigated in a single sample of the 2D quasicrystals, which is not possible in case of icosahedral quasicrystals exhibiting quasicrystalline ordering in all directions. In fact, some physical properties of decagonal quasicrystals show a strong anisotropy along the periodic and quasicrystalline directions [73].

Decagonal quasicrystals, which possess a unique 10-fold rotational axis along the periodic direction and two inequivalent sets of 2-fold axis perpendicular to the 10-fold axis (see Figure 1.4), are the most studied 2D quasicrystals because of the availability of thermodynamically stable, large, and high quality samples. A variety of periodicities has been observed along the 10-fold axis. Mainly, three groups of decagonal quasicrystals with a basic periodicity of 4 Å (Al-Co-Cu type), 12 Å (Al-Mn type), and 16 Å (Al-Fe-Pd type) have been found [77]. Decagonal Al-Ni-Co, the structure of which is discussed in this thesis, consists of two sets of quasicrystalline planes stacked alternately along the 10-fold axis. The distance between the planes is approximately 2 Å yielding a basic 4 Å periodicity [40, 64].

Al-Ni-Co alloys have attracted much attention due to the existence of various types of quasicrystalline and approximant structures observed in a wide composition range. They possess at least eight different types of quasicrystalline phases, namely basic Ni-rich (bNi), type I superstructure (I), S1 superstructure (S1), type II superstructure (II), basic Co-rich (bCo), one dimensional quasicrystal (1D), pentagonal (5f), and pentagonal with superstructure (5f_{HT}) (abbreviation after Ref. [78]). A cut through the phase diagram is shown in Figure 1.5. A brief

States	Periodicity	Tiling	Tiling Type
Basic Ni-rich	4 Å	pentagonal	perfect
S1 superstructure	8 Å	pentagonal	random
Type I superstructure	8 Å	rhombic	random
Type II superstructure	8 Å	pentagonal and rhombic	random
Basic Co-rich	8 Å	pentagonal	random
One dimensional	8 Å	pentagonal and rhombic	random
Pentagonal	8 Å	pentagonal	random
Pentagonal with superstructure	8 Å	rhombic	random

Table 1.1: Different phases of Al-Ni-Co with their periodicities and tiling.

explanation of some of these phases is presented here (refer to Ref. [78] for details).

Among the eight states listed, the first five show a diffraction pattern of 10-fold symmetry perpendicular to the periodic direction, while the pentagonal states possess a 5-fold symmetric diffraction pattern. The quasicrystalline ordering along one direction within the 10-fold plane transforms to crystalline ordering, forming a one dimensional quasicrystal state. As such, the 1D state is an intermediate state between the quasicrystalline and approximant phases. Both pentagonal and one dimensional states are closely related to the decagonal phases.

The HRTEM of the Ni-rich basic structure reveals that clusters of 20 Å diameter are located at the vertices of a perfect pentagonal Penrose tiling [54, 60, 61], while the clusters show some chemical disorder. In contrast, the cluster centers of the other phases form a random rhombic (Penrose) tiling of different variants and the clusters are chemically ordered.

Diffraction patterns of all phases except the basic Ni-rich structure show diffuse layers underneath the Bragg planes perpendicular to the periodic direction as well as half-way in between these planes, corresponding to an 8 Å periodicity [52, 79-84]. These diffuse layers are due to positional and orientational disorder of the columnar clusters [80, 85]. Other decagonal quasicrystals also exhibit such diffuse scattering [81, 86]. The intensity of the 8 Å periodic layers increases with increasing Co content and finally converts into sharp spots with quasicrystalline ordering. Different phases with their periodicities and tiling for the cluster centers are summarized in Table 1.1.

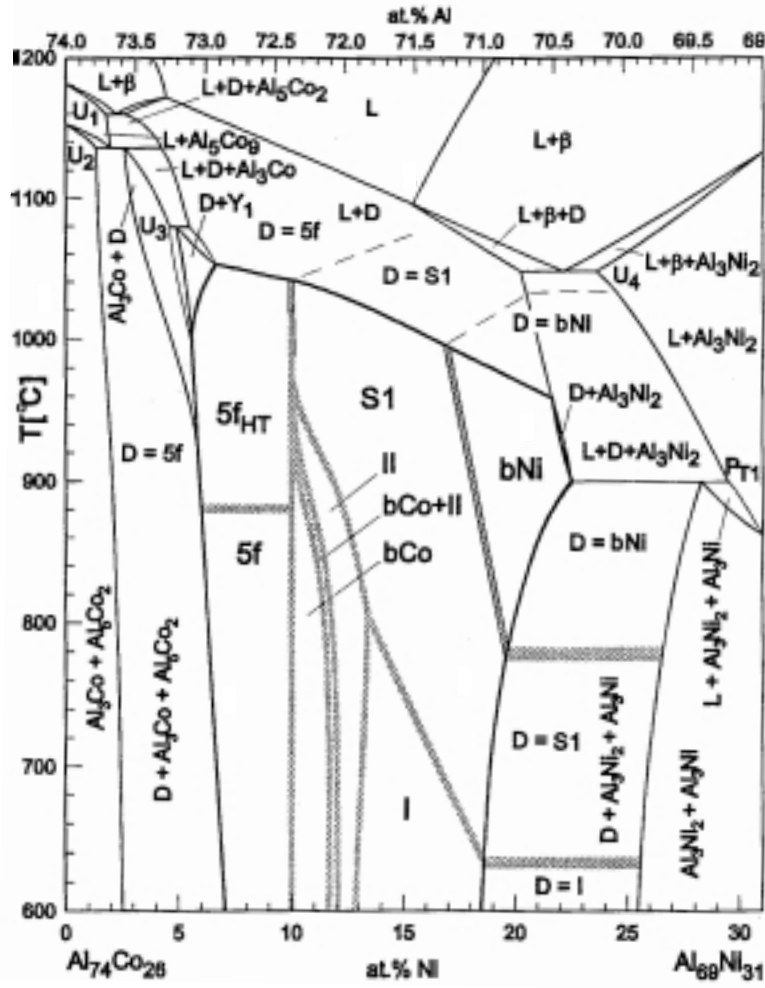


Figure 1.5: Phase diagram of Al-Ni-Co alloy from Ritsch *et al.* [78].

1.3.1 Indexing of the Diffraction Pattern

Five basis vectors are needed to generate a reciprocal lattice of decagonal quasicrystals. The diffraction vector \mathbf{H}^{\parallel} can be obtained by,

$$\mathbf{H}^{\parallel} = \sum_{j=1}^5 h_j \mathbf{b}_j, \quad (1.10)$$

where h_j are integers, $\mathbf{b}_j = b(\cos \frac{2\pi j}{5}, \sin \frac{2\pi j}{5}, 0)$ for $j = 1, \dots, 4$ and $\mathbf{b}_5 = b_5(0, 0, 1)$ with $b = |\mathbf{b}_j|$ ($j = 1, \dots, 4$) and $b_5 = |\mathbf{b}_5|$. The vectors \mathbf{b}_j ($j = 1, \dots, 4$) are the in-plane vectors pointing from the center to four vertices of a regular pentagon, while \mathbf{b}_5 is along the periodic direction (Figure 1.6).

A set of five indices $(h_1 h_2 h_3 h_4 h_5)$ is assigned to each diffraction spot. The set $(h_1 h_2 h_3 h_4 h_5)$ is called generalized Miller indices, which are used to label the orientation of lattice planes as in

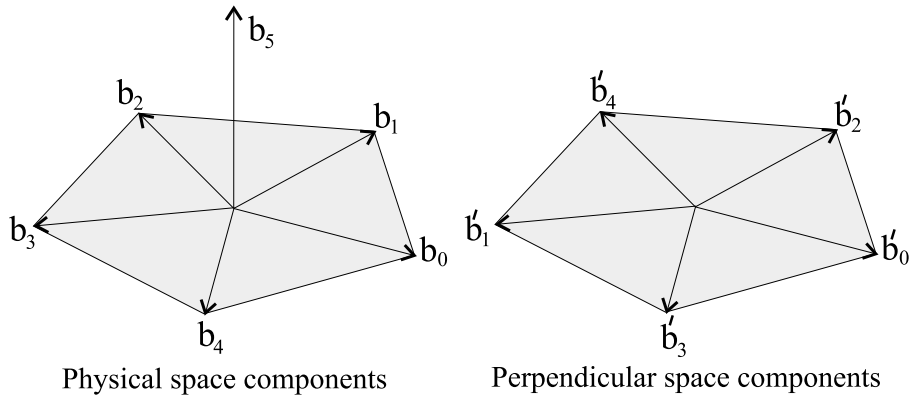


Figure 1.6: The projection of the 5D reciprocal basis vectors into the physical space (left) and perpendicular space (right).

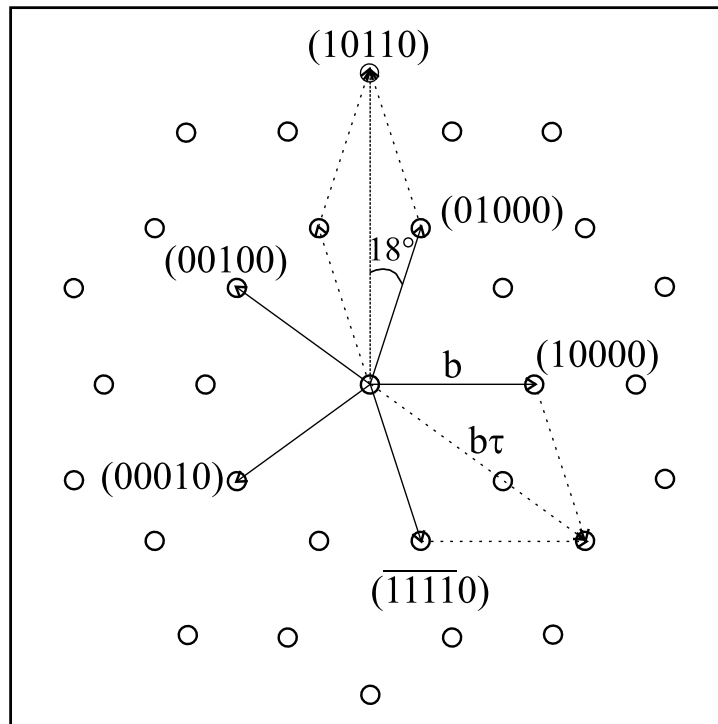


Figure 1.7: The indexing scheme of a decagonal quasicrystal. The circles denote the position of diffraction spots generated by $\mathbf{H}^{\parallel} = \sum_{j=1}^5 h_j \mathbf{b}_j$. The four of the five independent vectors $\mathbf{b}_j = b(\cos \frac{2\pi j}{5}, \sin \frac{2\pi j}{5}, 0)$ ($j = 1, \dots, 4$) shown by solid lines with arrow head are the in-plane basic vectors, while the fifth vector (00001) is along the periodic direction (here, perpendicular to the plane of the paper). The vector $(\bar{1}\bar{1}\bar{1}\bar{1}0)$ is sum of the four vectors \mathbf{b}_j ($j = 1, \dots, 4$) and not an independent basis vector.

the case of periodic crystals. The plane perpendicular to the vector [00001] has 10-fold symmetry and is referred as the (00001) plane. Similarly, the two inequivalent 2-fold planes perpendicular the vectors [10000] and [10110] are referred as (10000) and (10110) planes, respectively (see Figure 1.7). The vectors \mathbf{b}_j ($j = 1, \dots, 5$) can be regarded as the physical space projections of the reciprocal basis vectors \mathbf{d}_j^* ($j = 1, \dots, 5$) of a 5D periodic lattice given by,

$$\mathbf{d}_j^* = b \begin{pmatrix} \cos \frac{2\pi j}{5} \\ \sin \frac{2\pi j}{5} \\ 0 \\ \cos \frac{6\pi j}{5} \\ \sin \frac{6\pi j}{5} \end{pmatrix}, j = 1, \dots, 4; \quad \mathbf{d}_5^* = b_5 \begin{pmatrix} 0 \\ 0 \\ 1 \\ 0 \\ 0 \end{pmatrix}, \quad (1.11)$$

where b and b_5 are the lattice constants of the 5D space. The physical and perpendicular space projections of $\mathbf{d}_j^* = (\mathbf{b}_j, \mathbf{b}'_j)$ are shown in Figure 1.6.

1.3.2 Superstructure in *d*-Al-Ni-Co

As in periodic crystals, superstructure reflections in quasicrystals appear with weak intensity as compared to the intensity of main reflection. They are not indexable with integer indices with respect to the basis vectors of the main reflections. Several types of superstructures have been identified in both decagonal [87-89] and icosahedral quasicrystals [90]. Decagonal Al-Ni-Co phases exhibit three different types of superstructures: S1, type I, and type II. Decagonal $\text{Al}_{71.8}\text{Ni}_{14.8}\text{Co}_{13.4}$, which was investigated in this study, possesses the type I superstructure at room temperature.

For the type I superstructure, the physical space components \mathbf{s}_j of the reciprocal basis vectors of the 5D superlattice are rotated by $\frac{\pi}{10}$ and contracted by a factor $2 \cos \frac{\pi}{10}$ with respect to the physical space components of the normal basis vectors. They can be related by $\mathbf{b}_j = \sum_i S_{ij} \mathbf{s}_i$ with,

$$S = \begin{bmatrix} 1 & 0 & -1 & 0 & 0 \\ 0 & 1 & 0 & -1 & 0 \\ 1 & 1 & 2 & 1 & 0 \\ -1 & 0 & 0 & 1 & 0 \\ 0 & 0 & 0 & 0 & 1 \end{bmatrix}. \quad (1.12)$$

Since the determinant of the matrix S is 5, the reciprocal lattice spanned by \mathbf{s}_j , $\mathbf{H}^{\parallel} = \sum_j h_j^s \mathbf{s}_j$

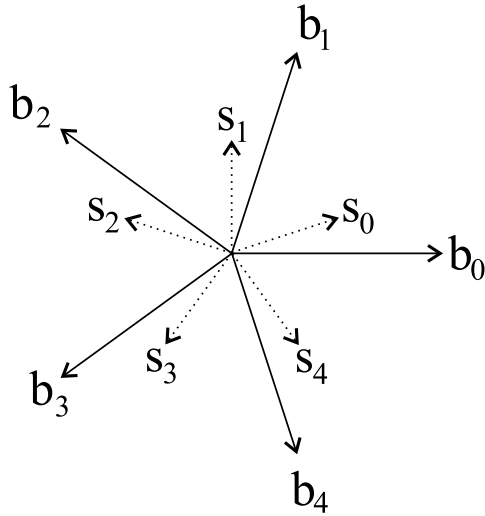


Figure 1.8: The physical space components of the normal and superstructure basis vectors of *d*-Al-Ni-Co.

can be divided into five sublattices satisfying the conditions $\sum_j h_j^s = 0$, $\sum_j h_j^s = \pm 1$, and $\sum_j h_j^s = \pm 2$. The sublattice with $\sum_j h_j^s = 0$ corresponds to the main reflections, while $\sum_j h_j^s = \pm 1$ and $\sum_j h_j^s = \pm 2$ represent superlattice reflections named S1 (first order) and S2 (second order) spots, respectively.

The type I superstructure phase exhibits both S1 and S2 spots, while the S1 superstructure state shows S1 spots and possibly much weaker S2 spots. The S1 spots appear around all strong reflections forming a decagon. Both S1 and S2 superstructure spots take $\frac{1}{5}$ -integer indices with respect to the basis vectors of the normal phase. At high temperature, the type I superstructure state undergoes a phase transition to the S1 superstructure state (see Figure 1.5).

Another type of superstructure observed in *d*-Al-Ni-Co is the so-called type II superstructure [89]. In this type, strong reflections are surrounded by a ring of pentagons. The pentagon is formed by five superstructure spots (new type, neither S1 nor S2) at the corners and a S1 spot at the center. The new spots are indexable with $\frac{1}{2}$ -integer indices with respect to the normal basis vectors.

1.3.3 Atomic Structure of *d*-Al-Ni-Co

The main building blocks of the *d*-Al-Ni-Co quasicrystals are columnar clusters. The cluster centers are located at the vertices of a periodic stacking of Penrose tilings. These cluster centers can be generated by decorating the unit cell of the 5D periodic lattice by atomic surfaces and taking the appropriate 3D cut.

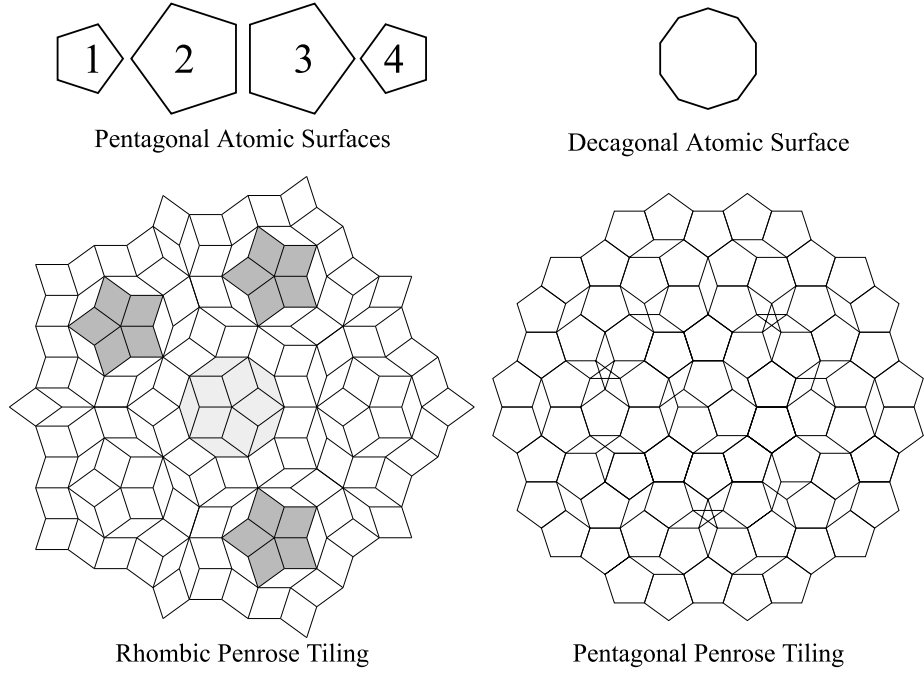


Figure 1.9: Penrose pattern generated by the section method, (a) Rhombic Penrose pattern and (b) Pentagonal Penrose pattern. Atomic surfaces of corresponding Penrose pattern are shown on the top of each pattern. Among the four pentagonal atomic surfaces, the smaller 1st and 4th have an equal radius of $\lambda_{1,4} = \frac{2}{5\tau^2 b}$. The radius of large pentagons (2nd and 3rd) is τ times larger than $\lambda_{1,4}$, i.e. $\lambda_{2,3} = \frac{2}{5\tau b}$. The 1st and 3rd pentagons have similar orientation and are related to the 2nd and 4th by inversion symmetry.

A model determining the structure of *d*-Al-Ni-Co proposed by Yamamoto *et al.* [66] is presented here, what successfully explains the observed superstructure (Type I). The model is based on the fact that clusters of 20 Å diameter are located at the vertices of a rhombic Penrose pattern of 20 Å edge length [66].

A rhombic Penrose pattern of edge length 20 Å can be generated by four types of pentagonal atomic surfaces (see Figure 1.9) located at the points $\pm(i,i,i,1.25)/5$ ($i = 1, 2$) of the 5D unit cell. The 5D basis vectors are given by,

$$\mathbf{d}_j = \frac{2}{5b} \begin{pmatrix} \cos \frac{2\pi j}{5} - 1 \\ \sin \frac{2\pi j}{5} \\ 0 \\ \cos \frac{6\pi j}{5} - 1 \\ \sin \frac{6\pi j}{5} \end{pmatrix}, j = 1, \dots, 4; \quad \mathbf{d}_5 = \frac{1}{b_5} \begin{pmatrix} 0 \\ 0 \\ 1 \\ 0 \\ 0 \end{pmatrix}, \quad (1.13)$$

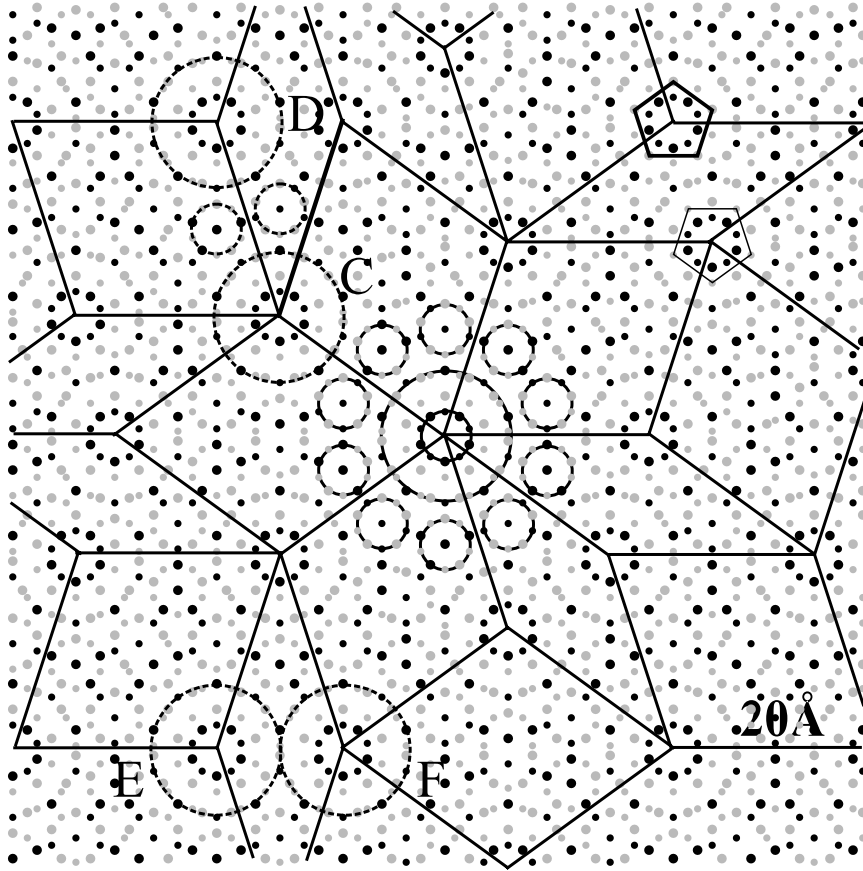


Figure 1.10: Atomic structure of d -Al-Ni-Co projected along the periodic direction obtained by the 5D superstructure model [66]. The clusters of 20 Å diameter are located at the vertices of a rhombic Penrose pattern of edge length 20 Å (solid lines). Dark and gray solid circles denote transition metals and Al, respectively. The large circles represent the atoms in the layer at $z = 0$ and the small circles at $z = c/2$.

where b^{-1} ($= 11.67$ Å) and b_5^{-1} ($= 4.081$ Å) are the lattice constants of the 5D lattice. The corresponding reciprocal basis vectors of \mathbf{d}_j are \mathbf{d}_j^* given by Equation 1.11.

The atom positions around the vertices of the Penrose tiling are generated by placing two independent occupation domains at 20 different points of the 5D unit cell (see Ref. [66] for details about occupation domains and their coordinates). The resulting atomic structure projected along the 10-fold axis is shown in Figure 1.10.

The structure is made up of two types of atomic layers with stacking sequences AB (A represents the layer at $z = 0$ and B the layer at $c/2$, with $c = 4$ Å (lattice constant along the periodic direction)). The cluster in each layer has pentagonal symmetry. The cluster in the

layer A is rotated by 36° with respect to the cluster in the layer B yielding an overall decagonal symmetry.

One of the columnar clusters projected along the 10-fold axis is marked by full circles in Figure 1.10. It consists of ten rings surrounding the inner wheel-like atomic arrangement. The neighboring two clusters overlap in two ways. First, they share the outer two rings (C and D) if the center-to-center distance is equal to the edge length of the Penrose pattern ($L = 20 \text{ \AA}$). Secondly, they share some of the atoms of the inner wheel (E and F) if the center-to-center distance is equal to the shorter diagonal of the skinny rhombus ($S = L/\tau = 12.36 \text{ \AA}$)

In the normal phase of *d*-Al-Ni-Co, the clusters are located at the vertices of a pentagonal Penrose tiling of 20 \AA edge length [66, and find references therein], while the atomic distribution in the cluster is the same for both phases. The pentagonal Penrose tiling can be generated from the 5D space decorated with a single decagonal atomic surface per unit cell as opposed to four pentagons for the case of the rhombic tiling [40]. The atomic positions of the normal phase are generated by two independent occupation domains, placed at 20 points of the 5D unit cell (refer to [66] for details).

The Diffraction Pattern

To calculate the diffraction patterns of the structures presented in the preceding section, a starting point is to evaluate the diffraction of the rhombic (and pentagonal) Penrose pattern. It can be obtained via the Fourier transform of the density distribution $\rho(\mathbf{r})$ of the 5D lattice decorated with pentagonal (and decagonal) atomic surfaces. The Fourier components of the 5D lattice can be separated into the product terms depending on the 3D physical space components and 2D perpendicular space components of the 5D reciprocal lattice vector. The physical space component contains the information of the usual atomic scattering factor and the temperature factor, while the perpendicular space components involve the Fourier transform of the atomic surfaces and the term describing the phason fluctuation.

The structure factor $F(\mathbf{H})$ is the Fourier transform of $\rho(\mathbf{r})$ and is expressed as [5],

$$F(\mathbf{H}) = \int_{UC} \rho(\mathbf{r}) e^{2\pi i \mathbf{H} \mathbf{r}} d\mathbf{r} = \sum_{k=1}^n T_k(\mathbf{H}) f_k(\|\mathbf{H}\|) e^{2\pi i \mathbf{H} \mathbf{r}_k}, \quad (1.14)$$

where the factor $f_k(\|\mathbf{H}\|)$ can be decomposed into the atomic scattering factor $f_k(\|\mathbf{H}^{\parallel}\|)$ and the Fourier transform of the atomic surface $g_k(\mathbf{H}^{\perp})$ (k denotes the atomic surface and runs from 1 to

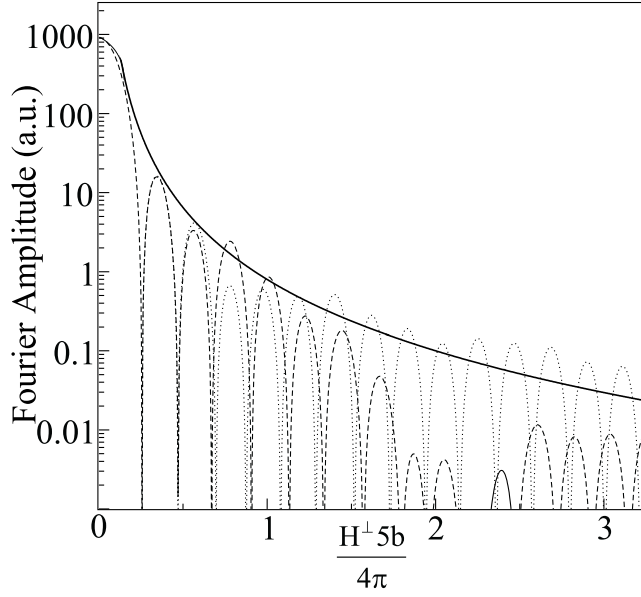


Figure 1.11: Fourier amplitude versus $\|\mathbf{H}^\perp\|$. The dotted- and dashed-curves represent the Fourier amplitudes along the high symmetry directions of the decagonal atomic surface, the solid curve is the envelop function. $\|\mathbf{H}^\perp\|$ is normalized by a lattice parameter b .

4 corresponding to the four pentagons for the rhombic Penrose pattern, while for the pentagonal Penrose pattern it has only one value $k = 1$ corresponding to the decagon). Similarly, the factor $T_k(\mathbf{H})$ can also be decomposed into the temperature and phason factor. Then Equation 1.14 can be rewritten as,

$$F(\mathbf{H}) = \sum_{k=1}^n T_k(\mathbf{H}^\parallel, \mathbf{H}^\perp) f_k(\|\mathbf{H}^\parallel\|) g_k(\mathbf{H}^\perp) e^{2\pi i \mathbf{H} \mathbf{r}_k}, \quad (1.15)$$

with

$$T_k(\mathbf{H}^\parallel, \mathbf{H}^\perp) = e^{-2\pi^2 \mathbf{H}^\parallel T \mathbf{B}^\parallel \mathbf{H}^\parallel} \times e^{-2\pi^2 \mathbf{H}^\perp T \mathbf{B}^\perp \mathbf{H}^\perp}, \quad (1.16)$$

(\mathbf{B} is the mean-square-displacement matrix), and

$$g_k(\mathbf{H}^\perp) = \frac{1}{A_{UC}^\perp} \int_{A_k} e^{2\pi \mathbf{H}^\perp \mathbf{r}^\perp} d\mathbf{r}^\perp, \quad (1.17)$$

(A_k is the area of k^{th} atomic surface and A_{UC}^\perp is the area of the 5D unit cell projected onto perpendicular space). A_{UC}^\perp is calculated by,

$$A_{UC}^\perp = \frac{4}{25b^2} \left[(7 + \tau) \sin \frac{2\pi}{5} + (2 + \tau) \sin \frac{4\pi}{5} \right]. \quad (1.18)$$

The Fourier transform of the pentagonal (or decagonal) atomic surface can be obtained by summing the Fourier transform of five (or ten) triangles forming the pentagon (or decagon).

Using the standard formula of the Fourier transform of a triangle, $g_k(\mathbf{H}^\perp)$ can be obtained by,

$$g_k(\mathbf{H}^\perp) = \frac{1}{A_{UC}^\perp} \sin \frac{2\pi}{5} \sum_{j=0}^m \frac{A_j(e^{iA_{j+1}\lambda_k} - 1) - A_{j+1}(e^{iA_j\lambda_k} - 1)}{A_j A_{j+1} (A_j - A_{j+1})} \quad (1.19)$$

where j runs over 5 (and 10) triangles of the pentagon (and decagon) and $A_j = 2\pi\mathbf{H}^\perp \mathbf{e}_j$ with,

$$\mathbf{H}^\perp = b \sum_j^m h_j \begin{pmatrix} 0 \\ 0 \\ 0 \\ \cos \frac{6\pi i}{5} \\ \sin \frac{6\pi i}{5} \end{pmatrix} \quad (1.20)$$

In the simplified case which excludes the effect of temperature and considers the identical atomic scattering factor, $f_k(\|\mathbf{H}\|)=1$, the intensity (I) depends only upon the Fourier transform of the atomic surfaces,

$$I \propto |g_k(\mathbf{H}^\perp)|^2 \quad (1.21)$$

The Fourier amplitudes of the decagonal atomic surface along the two high symmetry directions are shown in Figure 1.11. The envelope function of the Fourier amplitudes gives the average damping with \mathbf{H}^\perp . In principle, Fourier amplitudes corresponding to all \mathbf{H}^\perp contribute to the diffraction intensities and fill the reciprocal space infinitely densely. But the diffraction intensities for larger \mathbf{H}^\perp are extremely weak and are not experimentally detectable, which makes it possible to distinguish individual spots.

Until now, the diffraction pattern of the cluster centers is discussed without taking account of individual atoms in the cluster. To include the contribution of individual atoms, Fourier amplitudes of 20 occupation domains have to be considered, which modulate the intensity of diffraction spots but do not change their position.

The diffraction pattern obtained by the 5D superstructure model includes main, S1 and S2 spots (one can refer to Ref. [66] for the diffraction pattern). The intensity of the S2 spots is weaker than that of the S1 spots [91]. X-ray diffraction also shows that S2 spots are relatively weak [88].

Summary

Fundamental examples of quasiperiodic structure, the Fibonacci sequence and the Penrose pattern, were presented. The Fibonacci sequence illustrates quasiperiodic structure in 1D, the

Penrose tiling in 2D. These basic structures show discrete diffractions pattern without having periodicity demonstrating a long range order. The diffraction pattern of the Penrose pattern is very similar to the diffraction pattern observed in 2D quasicrystals. The section method to derive a quasicrystalline structure in physical space from higher dimensional periodic lattice was discussed. A simple example illustrating the generation of a Fibonacci sequence from a 2D periodic lattice was given. In addition, different models for the structure and the stability of quasicrystals were briefly discussed.

The phase diagram of Al-Ni-Co alloys was illustrated. Depending on temperature and exact alloy composition, Al-Ni-Co exhibits several different decagonal phases. Decagonal phases are 2D quasicrystals consisting of a periodic stacking of quasicrystalline planes along the 10-fold axis. The samples used in this work belong to the type I superstructure phase. As revealed by transmission electron microscopy, the structure of this phase can be explained in terms of a random tiling. Its diffraction pattern shows S1 and S2 superstructure spots. The atomic structure can be derived from a 5D decorated lattice and exhibits 20 Å diameter clusters located at the vertices of a rhombic Penrose tiling of 20 Å edge length.

The presented indexing scheme and other properties of the diffraction pattern of decagonal quasicrystals play an important role in the discussion of the experimental results of electron and He diffraction of the 10-fold *d*-Al-Ni-Co surface in Chapter 3. The tilings and clusters will be illustrated in scanning tunneling microscopy images of the same surface. The discussed features of the diffraction pattern of the Fibonacci lattice are reflected in the diffraction of the 2-fold *d*-Al-Ni-Co(10000) surface given in Chapter 4.